jet INTL JOURNAL OF ELECTRONICS AND TELECOMMUNICATIONS, 2022, VOL. 68, NO. 3, PP. 535-540
Manuscript received June 16, 2022; revised August, 2022. DOI: 10.24425/ijet.2022.141271

Reconstruction of Strains with a Non-smooth Distribution and Temperature Using Optical Fiber Bragg Grating

Małgorzata Detka, and Cezary Kaczmarek

***Abstract*—This paper presents a simulation study of the simultaneous reconstruction of the non-smooth strain distribution of an optical fiber Bragg grating and its temperature, which is based on the reflection spectrum of the reflected beam of the grating. The transition matrix method was used to model the reflection spectrum of the grating, and the nonlinear Nelder-Mead optimization method was used to simultaneously reconstruct the strain distribution along the grating and its temperature. The results of simulations of simultaneous reconstruction of the strain profile and temperature indicate good accord with the strain profiles and temperature set. The reconstruction errors of the strain profiles are less than 1.2 percent and the temperature change errors are less than 0.2 percent, with a noise level of 5 percent.**

***Keywords*—fiber Bragg grating; non-smooth strain distribution; reflection spectrum**

I. Introduction

FIBER optic sensors are currently used in many fields of technology, science, medicine and research due to their known advantages that conventional measurement sensors do not have. The development of sensor technology is still dynamic and is based on new optical fiber technologies, new optical fiber elements and new effects caused by physical and chemical quantities impacting the optical fiber or optical fiber element during light propagation. One direction of research in this area is to measure two or more quantities simultaneously using a single sensor. These sensors are called two-parameter or multi-parameter sensors, respectively. This usually uses different wavelengths and/or different modes of light for which the processing sensitivities of the measured quantities are different. The processing equation of a multi-parameter sensor written in matrix form, with the sensitivities of the measured quantities determined for different wavelengths or for different modes of light, allows the measured quantities to be reconstructed by calculating the inverse sensitivity matrix, subject to the condition that the determinant of the sensitivity matrix has a value different from zero. The most common two quantities measured simultaneously are strain and temperature [1,2], refractive index and temperature [3], fluid level and temperature [4], and force and temperature [5]. The most commonly simultaneously measured three quantities are torsion, strain and temperature [6]. The aforementioned multi-parameter sensors allow the realization of multi- or single-point measurements. Fiber-optic Bragg gratings make it possible to reconstruct estimates of their parameters and the measurand distribution functioning along their length based on their spectra. Many methods have been developed to implement the above inverse problem. Most commonly, the amplitude spectrum of the beam reflected by the grating and optimization methods are used for this purpose [7]-[10]. In [11], the authors used the Bragg grating amplitude spectrum and improved particle swarm optimization to simultaneously reconstruct the temperature and mean strain.

This paper presents a two-parameter sensor for simultaneous measurement of strain and temperature distribution based on the reflection spectrum of the reflected beam of a fiber optic Bragg grating. Simulation studies of the proposed sensor were performed. The transition matrix method was used to model the reflection spectrum of the grating, and the nonlinear Nelder-Mead optimization method was used to simultaneously reconstruct the strain distribution along the grating and its temperature. The results of simulations of simultaneous reconstruction of the strain profile and temperature indicate good accord with the strain profiles and temperature set. The reconstruction errors of the strain profiles are less than 1.2 % and the temperature change errors are less than 0.2 %, with a noise level of 5 %.

II. Method of Reconstructing the Strain Distribution and Temperature

There are two stages in the process of reconstructing the strain distribution and temperature change of the grating. In the first one, the amplitude spectrum of a uniform grating is calculated with given parameters, and then the grating parameters are reconstructed from the calculated amplitude spectrum after adding noise. In the next step, the amplitude spectrum of the grating subjected to the assumed strain distribution and temperature change is calculated using the previously reconstructed grating parameters, and then the strain distribution and temperature change are reconstructed based on the calculated spectrum and the addition of white noise.

To calculate the spectrum of the reflection beam of the uneven grating, the method of transition matrix was applied

M. Detka is with Faculty of Electrical Engineering, Automatic Control and Computer Science, Kielce University of Technology, Poland (e-mail: m.detka@tu.kielce.pl).

C. Kaczmarek is with Faculty of Electrical Engineering and Computer Science, Lublin University of Technology, Poland (e-mail: c.kaczmarek@pollub.pl).

[12]. For transparency of the paper, an outline of this method is given below.

The grating period, the changes of which are caused by the strain distribution $\varepsilon(z)$, and the temperature change ΔT can be expressed as:

$$\Lambda(z) = \Lambda_0[1 + (1 - p_e)\varepsilon(z) + (\alpha_1 + \alpha_n)\Delta T] \tag{1}$$

where Λ_0 is the initial period, and p_e the elasto-optic coefficient, z the distance along the longitudinal axis of the fiber, α_1 the temperature expansion coefficient of the optical fiber, and α_n the temperature-optic coefficient.

The distribution of the refractive index of the grating core characterizing the Bragg grating is a function:

$$n_{eff}(z) = n_0 + \delta n_{eff}(z)\cos(\frac{2\pi}{\Lambda}z + \varphi(z)) \tag{2}$$

where: n_o is the average value of the refractive index, δn_{eff} is the amplitude of variation of the refractive index, $\phi(z)$ describes the grating chirp.

If the grating is apodized with a Gaussian profile, the change in the refractive index is expressed by the formula:

$$\delta n_{eff}(z) = \delta n_{eff} \exp\left[-\rho\left(\frac{z - L/2}{L}\right)^2\right] \tag{3}$$

where L is the grating length, ρ is the parameter of Gaussian function width.

The mathematical model of a Bragg grating is a pair of coupled differential equations describing the interaction between two identical modes propagating in opposite directions [12].

In the transition matrix method, the grating is divided into M equal, uniform sections. Each section is described by a 2x2 transition matrix whose elements are a function of the optical wavelength, segment length, segment period, and physical properties of the grating. The period of each segment is calculated from relation (1) where $\varepsilon(z)$ and ΔT are local values. The $\boldsymbol{T}$ matrix describing the entire grating structure can be described by the equation:

$$\boldsymbol{T} = \boldsymbol{T}_M \cdot \boldsymbol{T}_{M-1} \cdot \ldots \cdot \boldsymbol{T}_k \cdot \ldots \cdot \boldsymbol{T}_1 = \begin{bmatrix} t_{11} & t_{12} \\ t_{21} & t_{22} \end{bmatrix} \tag{4}$$

where $\boldsymbol{T}_1$, $\boldsymbol{T}_2$ ... $\boldsymbol{T}_M$ are matrices of uniform sections *1*, *2* ... *M* of the grating. Relationships for the calculation of matrices of uniform sections are specified in [12, 13].

The power reflection coefficient for the whole grating takes on the form:

$$R = \left| -\frac{t_{21}}{t_{22}} \right|^2 \tag{5}$$

For the assumed values of the grating parameters L, Λ, δn_{eff}, ρ and $\varepsilon(z)$ and ΔT, based on the above relationships, it is possible to calculate the amplitude spectrum of the beam reflected by the grating.

The reconstruction of the strain profile and temperature changes, and the synthesis of the grating are performed using one of the optimization techniques: the Nelder-Mead simplex method [14]. The mean square deviation between the modeled and the reconstructed spectra of the grating is assumed to be the objective function:

$$f(\alpha) = \sqrt[4]{\int_0^\infty \left[R_{\mathrm{mod}}(\lambda) - R_{rec}(\lambda, \alpha_1, \ldots, \alpha_n)\right]^4 d\lambda} \tag{6}$$

where $R_{mod}(\lambda)$ and $R_{odt}(\lambda, \alpha_1, \ldots, \alpha_n)$ are the modeled and reconstructed spectra of the grating, respectively. By determining the minimum of the objective function $f(\alpha)$ we obtain optimal values of parameters $\alpha_1, \ldots, \alpha_n$.

III. SIMULATION RESULTS

In the first step of reconstructing the strain distribution and temperature changes of the grating, the parameters of the unstrained grating were reconstructed: L, Λ, δn_{eff}, ρ. For the assumed values of the grating parameters, the amplitude spectrum of the beam reflected by the grating, apodized with a Gaussian function (3) was calculated using the transition matrix method with the grating divided into 50 identical sections. White noise is added to the calculated spectrum. On the basis of the calculated amplitude spectrum, the grating parameters are reconstructed using the Nelder-Mead simplex algorithm with the objective function according to formula (6), where it is assumed that $\alpha_1 = L$, $\alpha_2 = \Lambda$, $\alpha_3 = \delta n_{eff}$, $\alpha_4 = \rho$.

In the second stage, the strain distribution and temperature change were reconstructed on the basis of its modelled spectrum caused by the set non-smooth strain distribution $\varepsilon(z)$ and the set temperature change ΔT. The grating strain was assumed to consist of a part of linearly increasing strain and a part of zero strain.

Strain distribution is a function:

$$\varepsilon(z) = \begin{cases} a(z - z_0) & dla \quad z \le z_0 \\ 0 & dla \quad z > z_0 \end{cases} \tag{7}$$

where z_0 is the point of the strain non-smoothness.

Given the determined grating parameters L, Λ, δn_{eff} and ρ the unknown parameters are now $\alpha_1 = a$, $\alpha_2 = \Delta T$, where a is the gradient of the nonzero part of the strain, and ΔT the change in grating temperature. Like in the first stage, the proposed method allows to determine the value of these two parameters, and thus it allows to reconstruct the non-smooth distribution of strain $\varepsilon(z)$ and grating temperature changes ΔT.

At this stage of the reconstruction, the assumed parameters of the grating are as follows: L = 10 mm, Λ = 530.834 nm, δn_{eff} = $26*10^{-5}$ and $\rho = 0.5$. The grating is also divided to 50 sections.

The assumed discontinuous strain distribution described by equation (7) in the practical implementation will be realized in a single-sided restrained beam with a constant cross-section with a fixed point of force application along its longitudinal axis. Both the coefficient of linear expansion of the carbon fiber beam itself and the grating were considered for temperature changes. The simulation was performed for compressive strain distributions in the range of 0-120 με/mm and temperature changes of 0 - 50 ºC at two noise levels of 2.5% and 5%. Figures 1, 2, 3 show the simulated and

reconstructed strain waveforms of the grating and the modeled and reconstructed spectrum of this grating for different temperature changes (ΔT = 0ºC, 10ºC, 20ºC, 30ºC) at a noise level of 2.5%, while in Figures 4, 5, 6 at a noise level of 5%. They show that the shape of these two spectra, as well as their central wavelengths are almost identical. These figures show that a partial strain of the grating induces a widening of the part of the grating's amplitude spectrum corresponding to its strained part. The strain induces a broadening of the shortwave portion of this spectrum. On the slopes of the widened parts of the spectrum, oscillations are observed. When a certain value of the strain gradient is exceeded, a splitting of the part of the spectrum corresponding to the strained part of the grating from the part of the spectrum corresponding to the non-strained grating occurs. These figures also show that a positive change in temperature shifts the spectrum into the longer wavelength range. The reconstruction errors of the strain and temperature distributions at the 2.5% noise level are shown in Tables I, II, III, and at the 5% noise level in Tables IV, V, VI. From the computational results presented, the reconstructions of both strain and temperature distributions were performed with high accuracy. The relative error of the strain gradient at a noise level of 2.5% does not exceed 0.6%. Grating temperature variations were reproduced much more accurately, with an error of less than 0.05%. However, at a noise level of 5%, the relative error of the strain gradient is less than 1.2% and the error in reproducing a change in temperature is less than 0.2%.

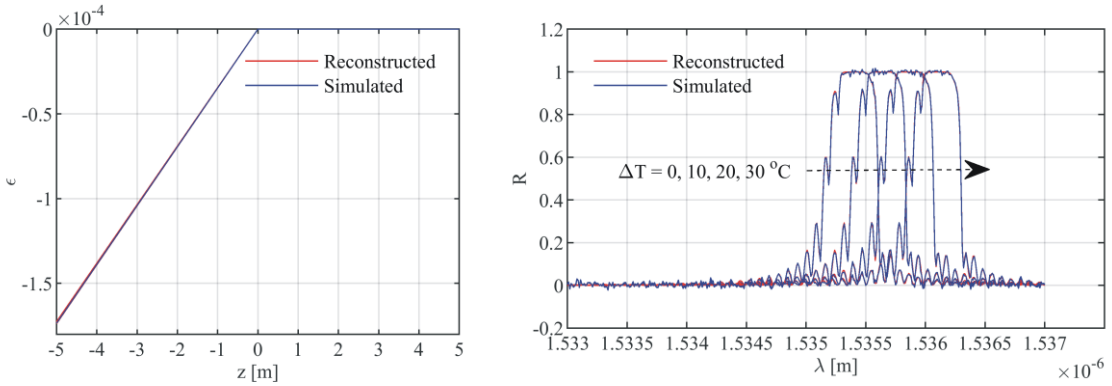

Fig.1. Simulated and reconstructed grating strain distribution with a gradient value of 34.72 με/mm and corresponding grating reflected beam spectra for different temperature increments ΔT, with a noise level of 2.5%

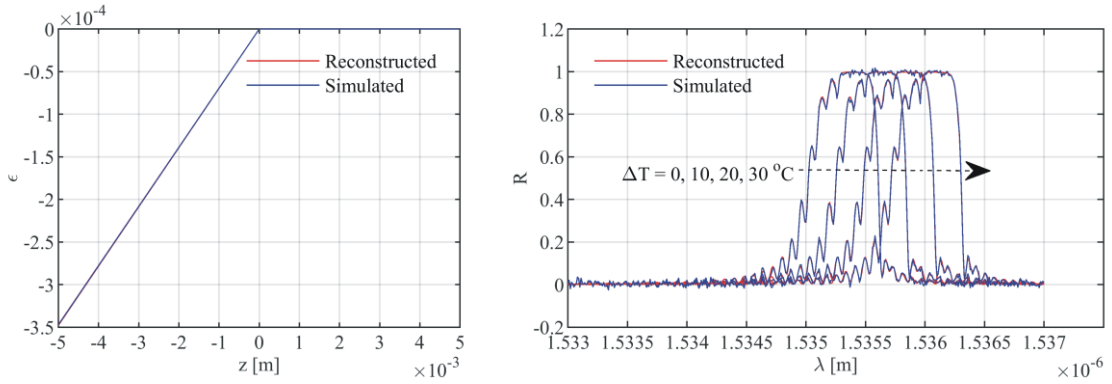

Fig.2. Simulated and reconstructed grating strain distribution with a gradient value of 69.44 με/mm and corresponding grating reflected beam spectra for different temperature increments ΔT, with a noise level of 2.5%

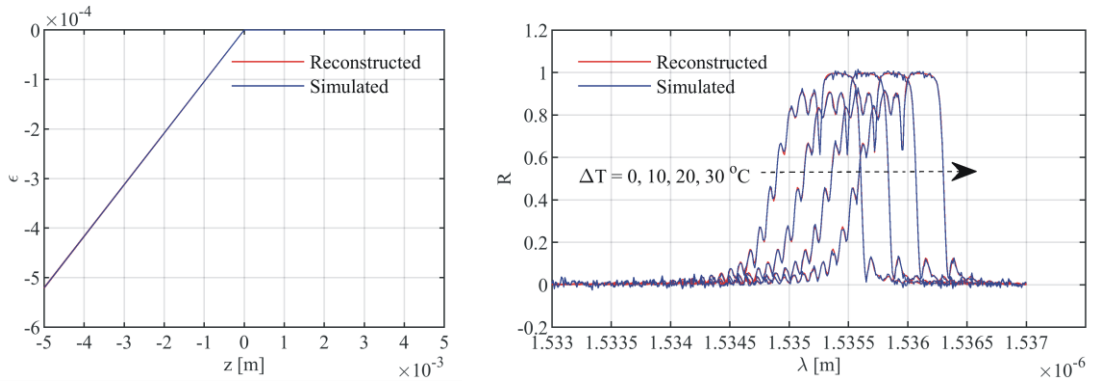

Fig.3. Simulated and reconstructed grating strain distribution with a gradient value of 104.16 με/mm and corresponding grating reflected beam spectra for different temperature increments ΔT, with a noise level of 2.5%

TABLE I
RECONSTRUCTION ERRORS OF STRAIN GRADIENT 34.72 με/MM AND RECONSTRUCTION ERRORS OF ΔT TEMPERATURE INCREMENTS AT A NOISE LEVEL OF 2.5%

Reconstructed gradient a values [με/mm]	Gradient error [%]	Set temperature increments ΔT [°C]	Reconstructed temperature increments ΔT [°C]	Temperature increments error [%]
34.77	0.14	0	$0{,}7*10^{-9}$	<0.01
34.55	0.49	10	10.003	0.03
34.64	0.24	20	20.001	<0.01
34.52	0.59	30	29.994	0.02

TABLE II
RECONSTRUCTION ERRORS OF STRAIN GRADIENT 69.44 με/MM AND RECONSTRUCTION ERRORS OF ΔT TEMPERATURE INCREMENTS AT A NOISE LEVEL OF 2.5%

Reconstructed gradient a values [με/mm]	Gradient error [%]	Set temperature increments ΔT [°C]	Reconstructed temperature increments ΔT [°C]	Temperature increments error [%]
69.57	0.19	0	$0{,}5*10^{-4}$	<0.01
69.439	<0.01	10	10.0006	<0.01
69.41	0.04	20	19.989	0.05
69.42	0.03	30	29.99	0.03

TABLE III
RECONSTRUCTION ERRORS OF STRAIN GRADIENT 104.16 με/MM AND RECONSTRUCTION ERRORS OF ΔT TEMPERATURE INCREMENTS AT A NOISE LEVEL OF 2.5%

Reconstructed gradient a values [με/mm]	Gradient error [%]	Set temperature increments ΔT [°C]	Reconstructed temperature increments ΔT [°C]	Temperature increments error [%]
104.03	0.12	0	$0{,}1*10^{-4}$	<0.01
104.33	0.16	10	10.001	0.02
103.997	0.16	20	20.008	0.04
104.29	0.12	30	30.006	0.02

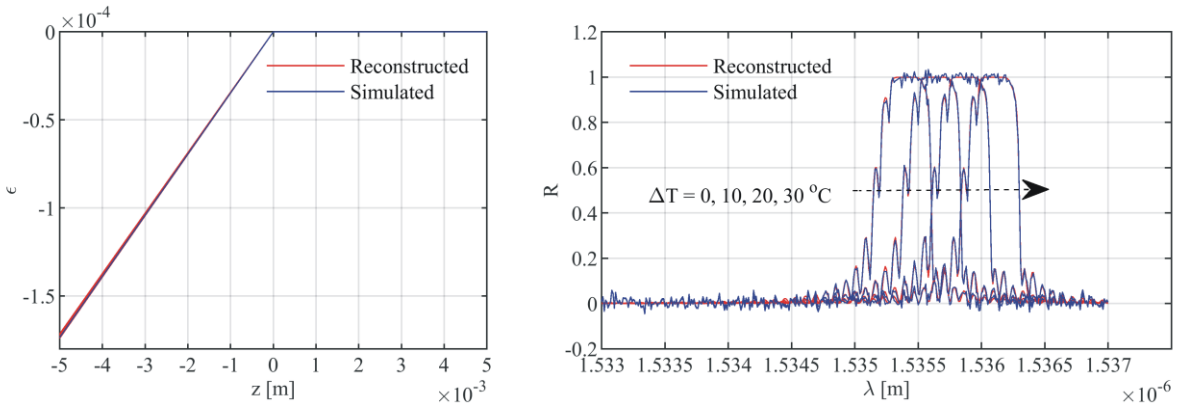

Fig.4. Simulated and reconstructed grating strain distribution with a gradient value of 34.72 με/mm and corresponding grating reflected beam spectra for different temperature increments ΔT, with a noise level of 5%.

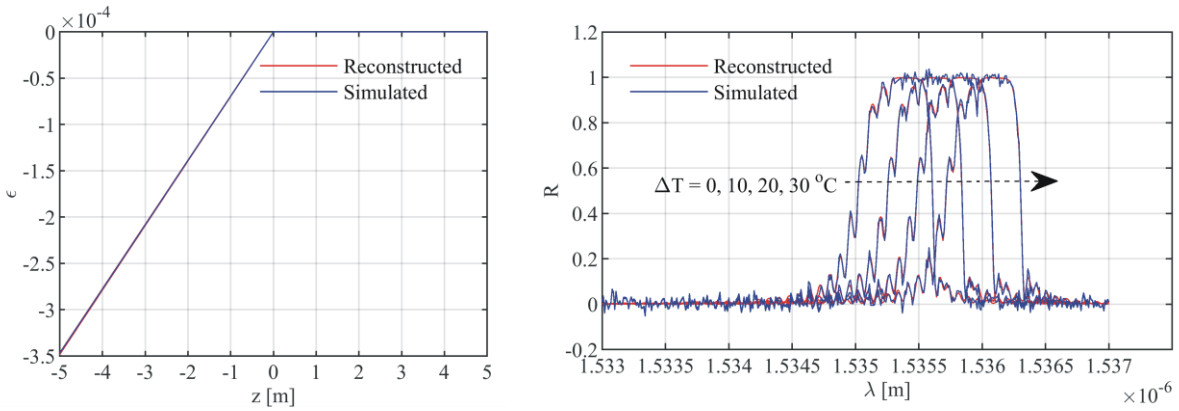

Fig.5. Simulated and reconstructed grating strain distribution with a gradient value of 69.44 με/mm and corresponding grating reflected beam spectra for different temperature increments ΔT, with a noise level of 5%.

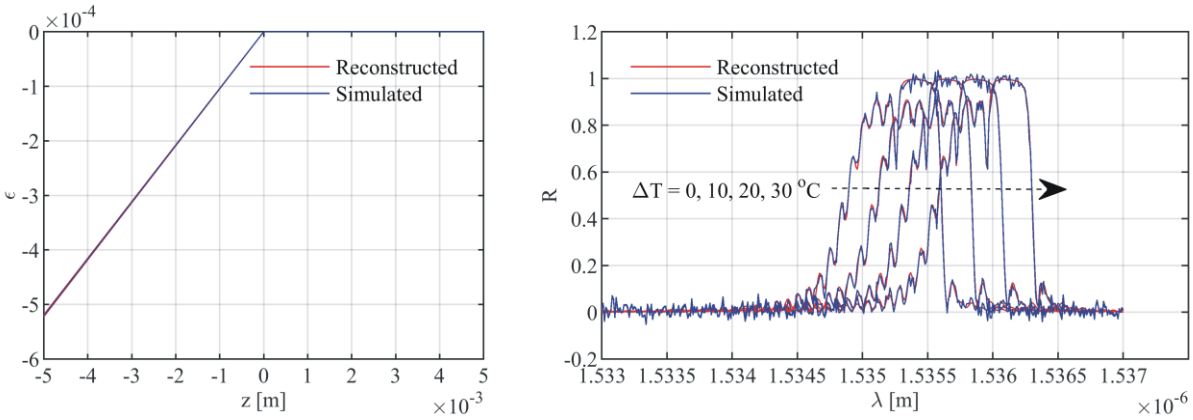

Fig.6. Simulated and reconstructed grating strain distribution with a gradient value of 104.16 με/mm and corresponding grating reflected beam spectra for different temperature increments ΔT, with a noise level of 5%.

TABLE IV
RECONSTRUCTION ERRORS OF STRAIN GRADIENT 34.72 με/MM AND RECONSTRUCTION ERRORS OF ΔT TEMPERATURE INCREMENTS AT A NOISE LEVEL OF 5%

Reconstructed gradient a values [με/mm]	Gradient error [%]	Set temperature increments ΔT [°C]	Reconstructed temperature increments ΔT [°C]	Temperature increments error [%]
34.81	0.27	0	$1{,}389*10^{-3}$	<0.01
34.39	0.96	10	10.006	0.06
34.55	0.49	20	20.003	0.02
34.31	1.19	30	29.988	0.04

TABLE V
RECONSTRUCTION ERRORS OF STRAIN GRADIENT 69.44 με/MM AND RECONSTRUCTION ERRORS OF ΔT TEMPERATURE INCREMENTS AT A NOISE LEVEL OF 5%

Reconstructed gradient a values [με/mm]	Gradient error [%]	Set temperature increments ΔT [°C]	Reconstructed temperature increments ΔT [°C]	Temperature increments error [%]
69.71	0.38	0	$-5{,}281*10^{-3}$	<0.01
69.43	0.015	10	10.001	0.01
69.37	0.10	20	19.979	0.10
69.39	0.07	30	29.979	0.06

TABLE VI
RECONSTRUCTION ERRORS OF STRAIN GRADIENT 104.16 με/MM AND RECONSTRUCTION ERRORS OF ΔT TEMPERATURE INCREMENTS AT A NOISE LEVEL OF 5%

Reconstructed gradient a values [με/mm]	Gradient error [%]	Set temperature increments ΔT [°C]	Reconstructed temperature increments ΔT [°C]	Temperature increments error [%]
103.90	0.255	0	$-2{,}525*10^{-3}$	<0.01
104.50	0.32	10	10.003	0.03
103.83	0.33	20	20.018	0.09
104.40	0.23	30	30.011	0.04

IV. CONCLUSION

This paper presents the application of the nonlinear Nelder-Mead optimization method and the transition matrix method to simultaneously reconstruct the non-smooth strain distribution of a fiber Bragg grating and its temperature, which are based on the intensity spectrum of the grating's reflected beam.

Numerical analysis of the spectral response of a fixed-period Bragg grating to an applied non-smooth strain shows that the strain gradient induces a broadening of the portion of the grating amplitude spectrum corresponding to the strained portion of the grating. On the slope of the widened parts of the spectrum, oscillations are observed. In addition, when a certain value of the strain gradient is exceeded, a splitting of the part of the spectrum corresponding to the strained part of the grating from the part of the spectrum corresponding to the non-strained grating occurs. It is also evident from the form of the

amplitude spectra that a positive change in the grating temperature causes the spectrum to shift into the longer wavelength range.

The simulations indicate that the reconstructions of both strain and temperature distributions were performed with high accuracy. The reconstruction errors of the strain profiles are less than 1.2 % and the temperature change errors are less than 0.2 %, with a noise level of 5 %.

The simulation results provide support for the conclusion that the Nelder-Mead optimization method can be successfully applied to simultaneously reconstruct the strain and temperature distributions of a grating using the amplitude spectrum of a fiber Bragg grating.

Further work will be focused on applying the proposed method to reconstruct the strain and temperature gradient from measured grating spectra subjected to non-smooth strain and temperature changes.

REFERENCES

[1] R. M. Andre, M. B. Marques, P. Roy, and O. Frazao, "Fiber loop mirror using a small core microstructured fiber for strain and temperature discrimination", *IEEE Photon. Technol. Lett*. 22 (15), 1120–1122 (2010).

[2] P. S. Reddy, R.L.N. Sai Prasad, D. Sen Gupta, M. Sai Shankar, K. Srimannarayana, U. Tiwwari, and V. Mishra, "A simple FBG sensor for strain-temperature discrimination", *Microw. and Opt. Technol. Lett*.. 53 (5), 1021–2024 (2011). https://doi.org/10.1002/mop.25901

[3] P. Liu, and Y. Shi, "Simultaneous measurement of refractive index and temperature using cascaded side-coupled photonic crystal nanobeam cavities", *Optics Express*, 25 (23), 28398–28406 (2017). https://doi.org/10.1364/OE.25.028398

[4] T. Osuch, T. Jurek, K. Markowski,and K. Jędrzejewski, "Simultaneous measurement of liquid level and temperature using tilted fiber Bragg grating", *IEEE Sensors J.*, 16 (5), 1205–1209 (2016). https://doi.org/10.1109/JSEN.2015.2501381

[5] Z. Yang, H. Xu, K. Ni, X. Dong, "Simultaneous measurement of force and temperature with a single FBG partially encapsulated with a metal canulla", *Microw. Opt. Technol. Lett.*, 53, 1656–1658 (2011). https://doi.org/10.1002/mop.26069

[6] L. Htein, D. S. Gunawardena, Z. Liu, and H-Y. Ibid., "Two semicircular-hole fiber in a Sagnac loop for simultaneous discrimination of torsion, strain and temperature", *Opt. Express*, 28 (23/9), 33841-33853 (2020). https://doi.org/10.1364/OE.402925

[7] M. Detka, "Reconstruction of strains with a non-smooth distribution using optical fiber Bragg grating", *Optical Fiber Technology*, 62 (9), (2021). https://doi.org/10.1016/j.yofte.2021.102466

[8] M. Detka, Z. Kaczmarek, "Distributed strain reconstruction based on a fiber Brag grating reflection spectrum", *Metrol Meas Syst.*, 20, 53-64 (2013). https://doi.org/10.2478/mms-2013-0005

[9] Ch. Song, J. Zhang, M. Yang, E. Shang and J. Zhang, "Reconstruction of fiber Bragg grating strain profile used to monitor the stiffness degradation of the adhesive layer in carbon fiber-reinforced plastic single-lap joint", *Advances in Mech. Eng.* 9 (3), 1-10, (2017). https://doi.org/10.1177/1687814016688575

[10] S. Zhang, N. Zhang, Y. Xia, H. Wang, "Research on non-uniform strain profile reconstruction along fiber Bragg grating via genetic programming algorithm and interrelated experimental verification", *Opt. Commun.*, 315, 338-346 (2014). https://doi.org/10.1016/j.optcom.2013.11.027

[11] Z. Wang, J. Wang, Q. Sui, L. Jia, "The simultaneous measurement of temperature and mean strain based on the distorted spectra of half-encapsulated fiber Bragg gratings using improved particle swarm optimization", *Opt. Commun.* 392, 153–161 (2017). https://doi.org/10.1016/j.optcom.2016.10.027

[12] Erdogan T., "Fiber grating spectra", *J. Lightwave Technol.* 15 (8), 1277-1294 (1997). https://doi.org/10.1109/50.618322

[13] Othonos T. A., Kalli K., "Fiber Bragg Grating: Fundamentals and Applications in Telecommunications and Sensing", *Artech House*, Boston, London, (1999).

[14] Lagaris J. C., Reeds J. A. Wright M. H., Wright P. E., "Convergence Properties of the Nelder-Mead Simplex Method in Low Dimensions", *Siam J., Optimizat.*, 9 (1), 112-147 (1998). https://doi.org/10.1137/S1052623496303470